

ON THE CORRELATION BETWEEN BIOMASS AND P-BAND POLARISATION PHASE DIFFERENCE, AND ITS POTENTIAL FOR BIOMASS AND TREE NUMBER DENSITY ESTIMATION

Maciej J. Soja, Erik Blomberg, and Lars M. H. Ulander

Chalmers University of Technology, 412 96 Gothenburg, Sweden

ABSTRACT

In this paper, a significant correlation between the HH-VV phase difference (polarisation phase difference, PPD) and the above-ground biomass (AGB) is observed for incidence angles above 30° in airborne P-band SAR data acquired over two boreal test sites in Sweden. A geometric model is used to explain the dependence of the AGB on tree height, stem radius, and tree number density, whereas a cylinder-over-ground model is used to explain the dependence of the PPD on the same three forest parameters. The models show that forest anisotropy need to be accounted for at P-band in order to obtain a linear relationship between the PPD and the AGB. An approach to the estimation of tree number density is proposed, based on a comparison between the modelled and observed PPDs.

Key words: polarisation phase difference (PPD) model, P-band, synthetic aperture radar (SAR), above-ground biomass (AGB), tree number density.

1. INTRODUCTION

In May 2013, the BIOMASS mission was selected by the European Space Agency (ESA) to become the first P-band SAR in space, with the main goal to map the global forests in terms of biomass, biomass change, and forest height [1]. Maps of forest parameters estimated with BIOMASS will find their use in climate modelling, disaster management, and the detection of deforestation and forest degradation.

During the BIOMASS feasibility study, the potential of P-band SAR for mapping of the aforementioned forest parameters was studied using data acquired with airborne SAR sensors. In boreal forests, three campaigns have been conducted: BioSAR 2007 [3] and 2010 [14]), conducted in Remningstorp, a hemi-boreal forest in non-topographic terrain in the south of Sweden, and BioSAR 2008 [2], conducted in Krycklan, a boreal forest in topographic terrain in the north of Sweden. The two test sites are separated by 720 km.

For boreal forests, biomass can be estimated with good accuracy from P-band SAR intensity data using a regression model based on the HV-polarised scattering coefficient, the HH/VV backscatter ratio, and the ground slope angle [10]. Moreover, the same model parameters can be used in both test sites, e.g., model parameters estimated in Krycklan can be used in Remningstorp, with a root-mean-square biomass estimation error of 22–33%. However, an overestimation of biomass is observed for forests with significant understorey vegetation. The understorey vegetation causes an increased cross-polarised backscatter without contributing significantly to the total biomass.

During a parallel study aiming at the development of a forward model for the BIOMASS End-to-End Simulator (BEES) [4, 11, 12], a significant correlation between the polarisation phase difference (PPD)

$$\Delta\Phi = \arg(S_{HH}S_{VV}^*) \quad (1)$$

and biomass was observed in BioSAR 2007 data ($R^2 \approx 0.62$). The observed correlation was not affected by understorey vegetation. Therefore, PPD may be potentially useful for biomass mapping. Also, as the PPD is one of the most basic polarimetric indicators, studies of PPD may improve the understanding of the scattering processes occurring in forests at P-band.

In this paper, the relationship between the PPD on the AGB is studied in airborne P-band SAR data acquired during the three BioSAR campaigns. Two theoretical models are proposed as possible tools explaining the dependence of the PPD on the AGB, both being functions of three basic forest parameters: tree height, stem diameter, and tree number density. AGB is modelled from these parameters using a simple geometrical model, whereas PPD is modelled using a cylinder-over-ground model, proposed earlier in [13]. A potential method for tree number density estimation is also proposed.

2. DATA

In this study, data acquired during the BioSAR campaigns are used. Three BioSAR campaigns have



Figure 1. Location of the two test sites used in the BioSAR campaigns.

been conducted in support of the BIOMASS feasibility study: two in Remningstorp in the south of Sweden (BioSAR 2007 and 2010) and one in Krycklan in the north of Sweden (BioSAR 2008). The test sites and the experimental data will now be briefly described.

2.1. Test Sites

Remningstorp is a hemi-boreal test site situated in southern Sweden ($58^{\circ} 28' N$, $13^{\circ} 38' E$). It is fairly flat with stand-level ground slopes lower than 5° (computed from a $50\text{ m} \times 50\text{ m}$ digital terrain model, DTM) [3, 7, 10, 14]. The test site covers approximately 1200 ha of productive forest land, and the forest consists primarily of Norway spruce (*Picea abies* (L.) Karst.), Scots pine (*Pinus sylvestris* L.), and birch (*Betula* spp.).

Krycklan is a boreal test site located in northern Sweden ($64^{\circ} 14' N$, $19^{\circ} 46' E$). Krycklan is situated 720 km north-north-east of Remningstorp. Unlike Remningstorp, Krycklan has a strongly undulating topography with stand-level ground slopes up to 19° (again, computed from a $50\text{ m} \times 50\text{ m}$ DTM) [2, 10]. The forest is dominated by Norway spruce and Scots pine.

The location of the test sites is shown in Fig. 1.

2.2. In situ and Lidar Data

In Remningstorp, two reference data sets are used. The first data set, used together with the BioSAR 2007 data, consists of ten $80\text{ m} \times 80\text{ m}$ plots, within which field measurements were conducted in autumn 2006 and spring 2007. Diameter at breast height (dbh) and tree species

were measured for all trees with dbh above 5 cm. For four plots, tree height and age were measured for all the calipered trees, whereas for the remaining six plots, tree height and age were measured only for a subset of the calipered trees. The exact sampling procedures are described in [3, 7, 10]. Biomass was estimated for each single tree from the sampled tree parameters using Marklund's species-specific allometric formulas [5], and tree-level biomass estimates were thereafter aggregated to plot-level biomass estimates.

The second data set in Remningstorp, used together with BioSAR 2010 data, consists of 32 circular, 0.5-hectare plots, of which seven are confined within the ten $80\text{ m} \times 80\text{ m}$ plots from the first data set in Remningstorp. During field measurements conducted in autumn 2010 and spring 2011, all trees with dbh higher than 5 cm were calipered and their species was determined. Tree height and age were measured for a subset of the calipered trees. The exact sampling procedures are described in [9]. Biomass was estimated from tree-level field measurements using the Heureka system [15].

In Krycklan, 31 stands of irregular shape and sizes between 2.4 and 26.3 hectares were inventoried in the summer of 2008. Systematic grids of circular field plots (radius 10 m) were laid out in each stand. The spacing of each grid was selected to give 8–13 field plots per stand. For each field plot, all trees with a dbh higher than 4 cm were calipered and the species was determined. Tree height and age were determined for a subset of the calipered trees. The exact sampling procedures are described in [2, 10]. Biomass was estimated from the field measurements using the Heureka system [15].

Lidar data were acquired in connection to each campaign. The acquired lidar data were used together with reference *in situ* data to create the biomass maps used in this paper. For a description of the biomass maps, consult [8, 10].

2.3. SAR Data

In Remningstorp, P-band SAR data were collected within the BioSAR 2007 campaign with the DLR E-SAR sensor during three different periods of spring 2007: 3rd of March, 31st March to 2nd of April, and 2nd of May [3]. At each occasion, two flight headings were used for P-band: 179° and 200° relative north. The first track features steeper incidence angles for all stands, close to those expected for a spaceborne scenario (all 10 plots lie in near range with nominal incidence angles between 26° and 35°). The second track features a wider range of incidence angles (between 30° and 50°).

On the 23rd of September 2010, both tracks of the BioSAR 2007 campaign were re-flown within the BioSAR 2010 campaign with the ONERA SETHI system, and a new track covering all 10 plots was added, acquired at heading 271° and with a similar range of incidence angles as for the 200° heading.

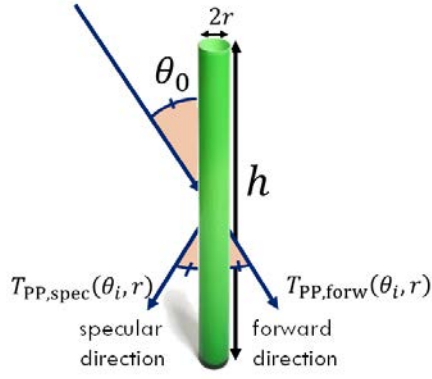


Figure 2. Scattering geometry for one cylindrical tree trunk.

In Krycklan, P-band SAR data were acquired between 14th and 15th of October 2008 within the BioSAR 2008 campaign. On the first day, two tracks were flown (134° and 314°), covering the same area from two directions. On the second day, SAR data of a smaller area were collected from four directions (headings: 43° , 134° , 314° , and 358°). In total, four unique headings were flown. For all acquisitions, the incidence angles were in similar range as for the acquisitions made at the 200° and 271° headings in Remningstorp.

3. MODELS

Two models are used in this paper. A geometrical model is used to explain the main dependence of the above-ground biomass (AGB) on three basic geometrical forest parameters: stem radius, tree height, and tree number density. A cylinder-over-ground scattering model is used to predict the polarisation phase difference from the same three forest parameters. The two models will now be briefly described.

3.1. Biomass Model

A simple geometrical model is obtained under the assumption that a forest plot consists of N identical trees per hectare, all with stem radii r and tree heights h :

$$\text{AGB}_{\text{mod}} = CNr^2h \quad (2)$$

where

$$C = \pi F \rho B$$

is a forest type-dependent constant, being a product of a taper factor F (accounting for the non-cylindrical stem shape), dry wood density ρ (converting stem volume to dry stem mass), and biomass expansion factor B (accounting for biomass of branches and needles/leaves).

3.2. Phase Difference Model

In this paper, a polarisation phase difference model previously proposed in [13] is used. The model assumes that the double-bounce interaction between tree trunks and the ground is the dominant scattering mechanism, the volume of tree trunks is a low-loss medium, the ground can be modelled as a flat, horizontal dielectric surface, and the trunks can be modelled as vertical, tapered, infinite dielectric cylinders.

In [13], three contributions are modelled separately and summed:

$$\Delta\Phi = \underbrace{\Delta\Phi_{\text{gr}} + \Delta\Phi_{\text{tr}}}_{\text{double bounce effect}} + \underbrace{\Delta\Phi_{\text{p}}}_{\text{propagation}}, \quad (3)$$

where:

- $\Delta\Phi_{\text{gr}}$ is the phase difference introduced by the reflection from the ground,
- $\Delta\Phi_{\text{tr}}$ is the phase difference introduced by the reflection from the tree trunks,
- $\Delta\Phi_{\text{p}}$ is the phase difference introduced by the different propagation delays for the H- and V-polarised fields in a volume of thin vertical cylinders.

Next, each contribution will be discussed separately. The scattering geometry is depicted in Fig. 2.

3.2.1. Ground Reflection

Phase difference due to ground reflection is modelled from the Fresnel reflection coefficients:

$$\Delta\Phi_{\text{gr}} = \Delta\Phi_{\text{gr}}(\theta_0) = \arg[R_{\text{H}}(\theta_0) \cdot R_{\text{V}}^*(\theta_0)], \quad (4)$$

where

$$R_{\text{H}}(\theta_0) = \frac{\cos\theta_0 - \sqrt{\varepsilon_{\text{gr}} - \sin^2\theta_0}}{\cos\theta_0 + \sqrt{\varepsilon_{\text{gr}} - \sin^2\theta_0}}$$

and

$$R_{\text{V}}(\theta_0) = \frac{\sqrt{\varepsilon_{\text{gr}} - \sin^2\theta_0} - \varepsilon_{\text{gr}} \cos\theta_0}{\sqrt{\varepsilon_{\text{gr}} - \sin^2\theta_0} + \varepsilon_{\text{gr}} \cos\theta_0}$$

are the Fresnel reflection coefficients for the horizontally (H) and vertically (V) polarised fields, respectively. The Fresnel reflection coefficients are dependent on the incidence angle θ_0 (as well as the dielectric coefficient for the ground ε_{gr}), but they are not affected by forest properties. Therefore, the correlation between the PPD and the AGB cannot be introduced by this term.

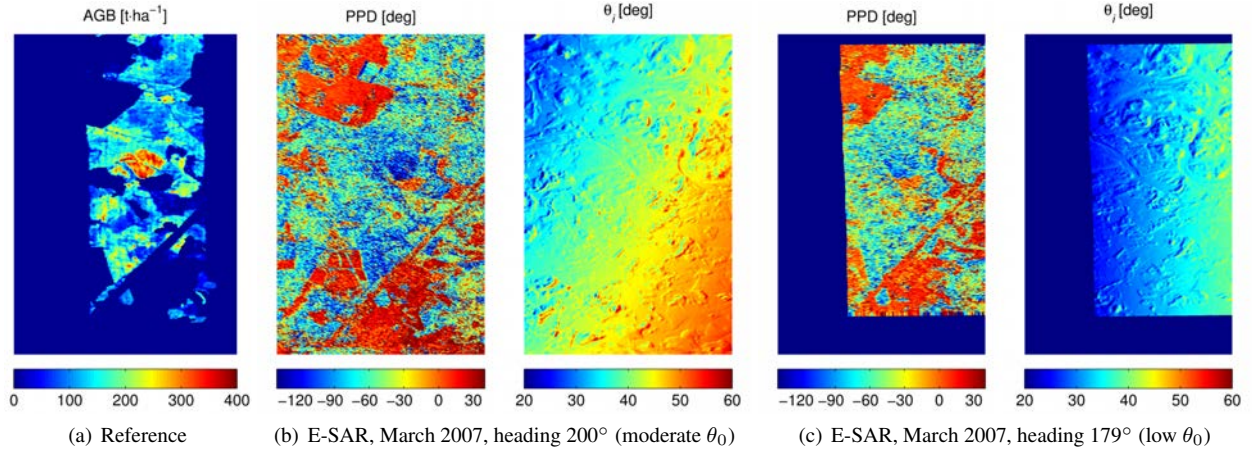


Figure 3. A comparison between a reference biomass map and polarisation phase difference and local incidence angle maps for two acquisitions over Remningstorp made during the BioSAR 2007-campaign with the DLR E-SAR system.

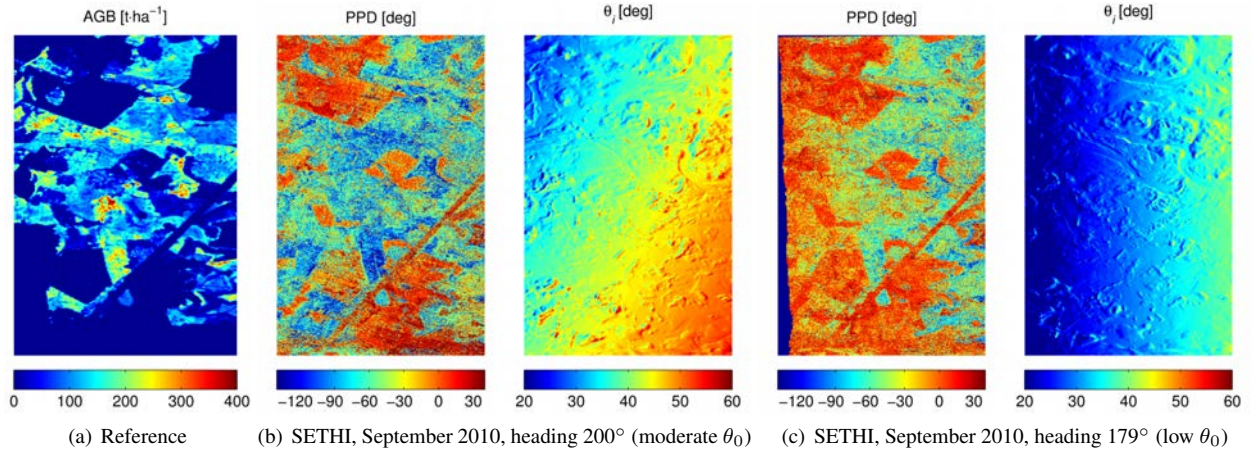


Figure 4. A comparison between a reference biomass map and polarisation phase difference and local incidence angle maps for two acquisitions over Remningstorp made during the BioSAR 2010-campaign with the ONERA SETHI system.

3.2.2. Trunk Reflections

Phase difference due to trunk reflections is modelled using the truncated infinite cylinder approximation:

$$\begin{aligned} \Delta\Phi_{\text{tr}} &= \Delta\Phi_{\text{tr}}(\theta_0, r) \\ &= \arg [T_{\text{H,spec}}(\theta_0, r) \cdot T_{\text{V,spec}}^*(\theta_0, r)], \end{aligned} \quad (5)$$

where

$$T_{\text{H,spec}}(\theta_0, r) = \sum_{n=-\infty}^{\infty} (-1)^n C_n^{\text{TE}}(\theta_0, r)$$

and

$$T_{\text{V,spec}}(\theta_0, r) = \sum_{n=-\infty}^{\infty} (-1)^n C_n^{\text{TM}}(\theta_0, r)$$

are the normalised far-field amplitudes in the specular direction (see Fig. 2), and $C_n^{\text{TM}}(\theta_0, r)$ and $C_n^{\text{TE}}(\theta_0, r)$ are

given by equations (4.2-36) and (4.2-37) in [6] (where $\Psi = 90^\circ - \theta_0$, $\mu_r = 1$, $a_0 = r$, $\epsilon_r = \epsilon_{\text{tr}}$, and k_0 is the wavenumber in vacuum).

For the chosen truncated infinite cylinder approximation, the far-field amplitudes $T_{\text{H,spec}}$ and $T_{\text{V,spec}}$ will be functions of the radius r of the tree trunk and the incidence angle θ_0 (as well as the dielectric coefficient for the tree trunk ϵ_{tr}). The phase shift introduced by trunk reflections will therefore be independent of the number of the trees and the height of the forest.

3.2.3. Propagation Through Layer of Vertical Cylinders

In [13], this contribution is modelled by replacing the volume of vertical cylinders with an equivalent low-loss anisotropic medium. The phase shift is then computed

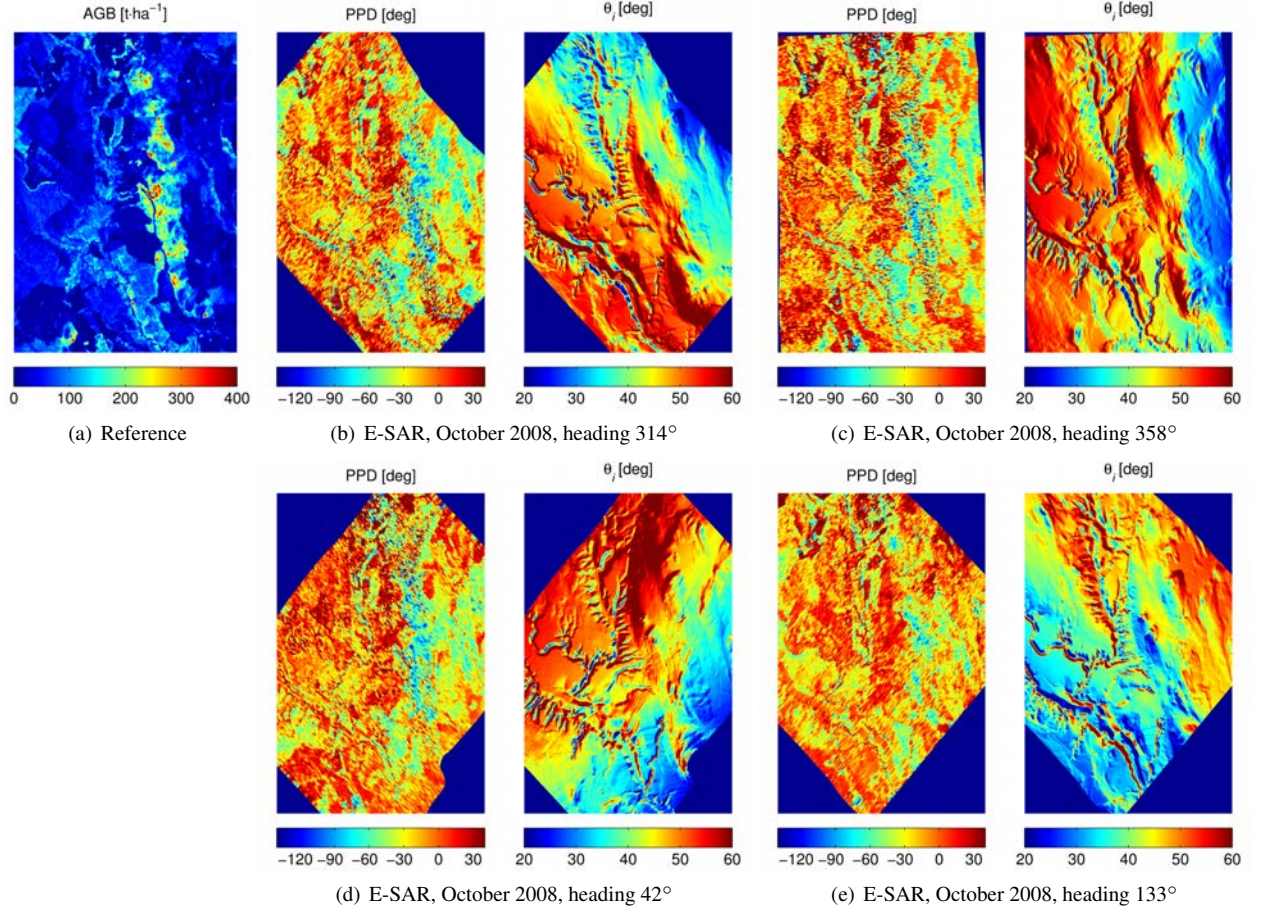


Figure 5. A comparison between a reference biomass map and polarisation phase difference and local incidence angle maps for four acquisitions over Krycklan made during the BioSAR 2008-campaign with the DLR E-SAR system.

from the attenuations for the H- and V-polarised waves. For each polarisation, the attenuation is computed from the far-field amplitude in the forward direction. The phase shift due to different effective propagation velocities in the anisotropic volume is:

$$\begin{aligned} \Delta\Phi_p &= \Delta\Phi_p(N, h, \theta_0, r) \\ &= Nh f_p(\theta_0, r), \end{aligned} \quad (6)$$

where

$$f_p(\theta_0, r) = \frac{4}{k_0} \{ \text{Im} [T_{H, \text{forw}}(\theta_0, r)] - \text{Im} [T_{V, \text{forw}}(\theta_0, r)] \}$$

is a propagation factor, dependent on the incidence angle θ_0 and trunk radius r (and the dielectric constant of the tree trunk). As it can be observed in (6), the phase difference is a linear function of the tree number density N and tree height h . The normalised far-field amplitudes in the forward direction are computed using:

$$T_{H, \text{forw}}(\theta_0, r) = \sum_{n=-\infty}^{\infty} C_n^{\text{TE}}(\theta_0, r)$$

and

$$T_{V, \text{forw}}(\theta_0, r) = \sum_{n=-\infty}^{\infty} C_n^{\text{TM}}(\theta_0, r).$$

4. RESULTS AND DISCUSSION

In this section, the PPD observed in BioSAR data will be studied against AGB estimates obtained from *in situ* and lidar measurements. Thereafter, the proposed models will be used to explain the observations.

4.1. Correlation Between PPD and AGB

In Figs. 3–5, the PPD is shown together with the local incidence angle θ_i (measured as the angle between the incidence direction and a surface normal for a 10 m × 10 m lidar DTM) and compared to reference AGB maps obtained using *in situ* and lidar data. A negative correlation between AGB and PPD is observed for most acquisitions except those made at steep incidence angles, like in Fig. 3(c) and Fig. 4(c). Moreover, it is observed in acquisitions over Krycklan made from different headings that the influence of ground slope is quite low, see Fig. 5. This is due to the fact that the polarisation phase difference is determined by the strongest scattering mechanism, which in general is a double-bounce interaction between a hori-

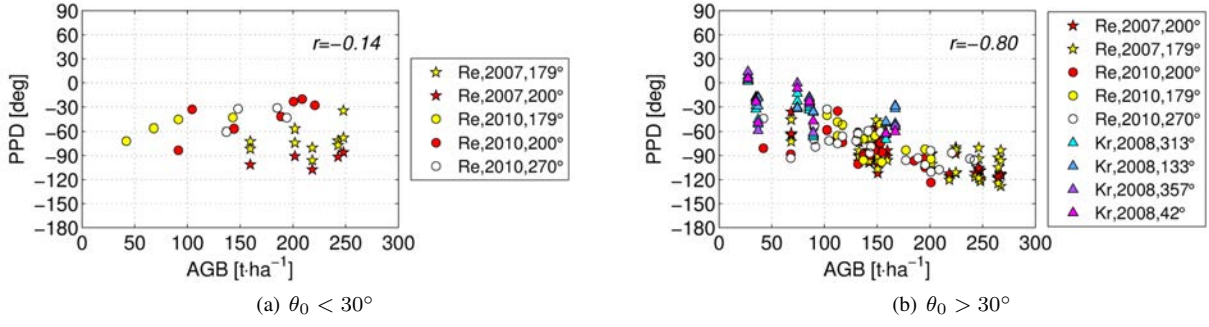


Figure 6. Stand- and plot-level estimates of PPD plotted against the AGB.

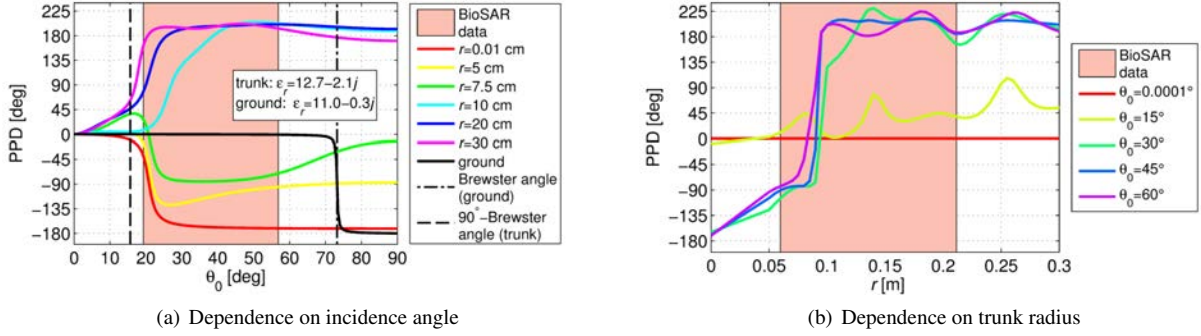


Figure 7. Dependence of the phase difference introduced by trunk and ground reflections on the incidence angle and the trunk radius.

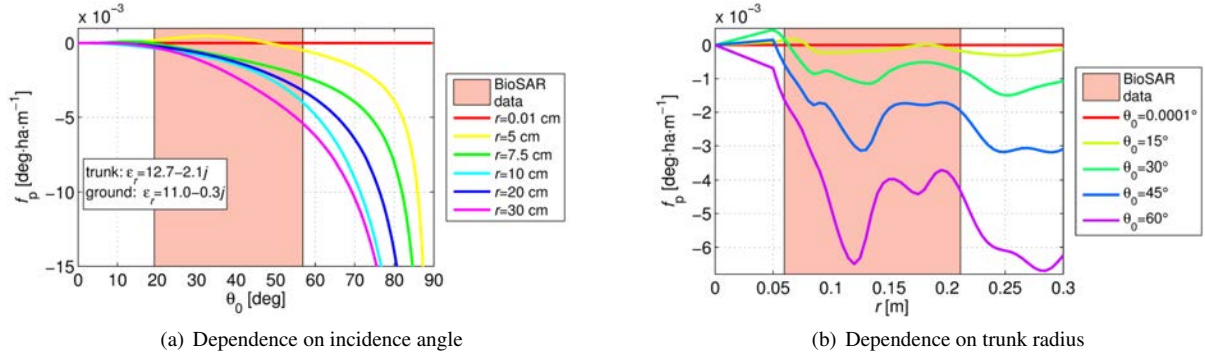


Figure 8. Dependence of the propagation factor on the incidence angle and the trunk radius.

zontal ground surface and a vertical tree trunk. Additionally, the temporal stability is good, as it is observed for acquisitions from BioSAR 2007 and 2010, see Fig. 3 and Fig. 4.

In Fig. 6, plot- and stand-level estimates of PPD are plotted against AGB for two cases: low incidence angles ($\theta_0 < 30^\circ$) and high incidence angles ($\theta_0 > 30^\circ$). It is observed that the correlation is low for incidence angles below 30° (Pearson correlation coefficient $r_P = -0.14$). For incidence angles above 30° , the correlation is significant (Pearson correlation coefficient $r_P = -0.80$). The

following empirical model is motivated:

$$\widehat{\Delta\Phi} = a(\theta_0) + b(\theta_0) \cdot \widehat{AGB} + \epsilon \quad (7)$$

where ϵ is a zero-mean error term and $a(\theta_0)$ and $b(\theta_0)$ are model parameters, which are functions of the incidence angle.

4.2. Agreement Between Observations and Theory

In Fig. 7, the phase shifts due to specular ground and trunk reflections are studied against the incidence angle

and trunk radius. It can be observed that the phase difference due to ground reflection is 0° up to approximately the Brewster angle for the ground surface. Above that, the phase difference changes with 180° . For the trunk reflection, the phase difference is close to 0° for low incidence angles, but it changes to approximately 180° when the incidence angle exceeds the complementary angle to the Brewster angle for the trunk. For large radii ($r > 10$ cm), the phase difference appears independent of radius. Note that a resonant behaviour can be observed in the plots. In real applications, trunk radii are distributed within a plot and the resonance effects are diminished. Summarising, it is observed that the sum $\Delta\Phi_{\text{gr}} + \Delta\Phi_{\text{tr}}$ is close to 180° for large r and moderate θ_0 , and therefore independent of trunk size. Note that for a dihedral corner reflector, the phase shift is 180° , which agrees with the observations in Fig. 7.

In Fig. 8, the propagation factor f_p is studied against the incidence angle and trunk radius. It is observed that the phase difference due to different propagation delays increases with both r and θ_0 . A resonant behaviour is also observed, but, similarly to the case of the cylinder reflection, the resonance effects will be diminished in real applications due to size distribution of cylinders within a plot. It is reasonable to conclude that f_p can be approximated as a product of two functions, one of r and one of θ_0 , meaning that a change of the incidence angle only affects the scaling.

Based on the observations made in the last two paragraphs, the following two conclusions are drawn:

- $\Delta\Phi_{\text{gr}}(\theta_0) + \Delta\Phi_{\text{tr}}(\theta_0, r) \approx C$ for large r and moderate θ_0 ,
- $f_p(\theta_0, r) \approx f_{p,1}(\theta_0)f_{p,2}(r)$.

Using these observations in the PPD model (3) yields:

$$\begin{aligned} \Delta\Phi_{\text{mod}} &= \Delta\Phi_{\text{gr}}(\theta_0) + \Delta\Phi_{\text{tr}}(\theta_0, r) \\ &\quad + Nh f_p(\theta_0, r) \\ &\approx C + f_{p,1}(\theta_0)f_{p,2}(r)Nh. \end{aligned} \quad (8)$$

If $f_{p,2}(r)$ can be approximated by a quadratic function of r , the AGB model (2) can be used, and the right-hand-side of (8) will have the same functional form as the empirical model (7) obtained from BioSAR data. The general shape of the curves in Fig. 8(b) shows that a quadratic dependence of $f_{p,2}(r)$ on r is reasonable. This hints that the propagation term in (3) may be responsible for the observed correlation between the PPD and the AGB, which implies that anisotropy may be an important effect to consider in scattering models for forests at P-band.

4.3. Estimation of Tree Number Density

Tree number density N can be estimated from experimental data by comparing the observed PPD with the modelled PPD. As h , forest height estimated using, e.g.,

PolInSAR height inversion can be used, while an allometric relation can be used to compute stem radius r from height. Dielectric constants can be approximated using known values for given forest types and soils. Tree number density can then be estimated using:

$$\hat{N} = \frac{\widehat{\Delta\Phi} - [\Delta\Phi_{\text{gr}}(\theta_0) + \Delta\Phi_{\text{tr}}(\theta_0, r(\hat{h}))]}{\hat{h}f_p(\theta_0, r(\hat{h}))}, \quad (9)$$

where \hat{h} is a forest height estimate and $r(\hat{h})$ is an allometric function for stem radius estimation from forest height.

5. CONCLUSIONS AND FUTURE PROSPECTS

In this paper, a correlation between the above-ground biomass (AGB) and the polarisation phase difference (PPD), i.e., the phase difference between the HH- and VV-channels, is observed in airborne P-band SAR data acquired during the three BioSAR campaigns over two boreal test sites in Sweden. To explain the observed relation, a theoretical model for the PPD is used, based on the assumption that forest scattering is dominated by the double-bounce effect and including a phase shift due to different propagation delays for the H- and V-polarised fields. In connection with a geometrical model for the AGB, the PPD model can explain the observed linear relationship between the PPD on the AGB only if forest is treated as an anisotropic medium.

The observed correlation is significantly lower for incidence angles below 30° . Although this is not optimal for future use with BIOMASS data (for which $\theta_0 \approx 25^\circ$), further studies are needed to better understand the dependence of the polarisation phase difference on biomass. Future development of the model includes modelling of topographic effects, simulating stem parameter distribution within plot (in terms of dimensions and dielectric properties), adding stem tapering, and connecting the model with the experimental data.

ACKNOWLEDGMENTS

The authors would like to thank ESA for the BioSAR data and SLU for the reference data.

REFERENCES

- [1] ESA (2012). *Report for Mission Selection: BIOMASS*. ESA SP-1324/1 (3 volume series), European Space Agency, Noordwijk, The Netherlands.
- [2] I. Hajnsek, R. Scheiber, M. Keller, R. Horn, S. Lee, L. M. H. Ulander, A. Gustavsson, G. Sandberg, T. Le Toan, S. Tebaldini, A. M. Guarnieri, and F. Rocca. BioSAR 2008 technical assistance for the

- development of airborne SAR and geophysical measurements during the BioSAR 2008 experiment: Final report – BioSAR campaign. Technical report, ESA contract no. 22052/08/NL/CT, 2009.
- [3] I. Hajnsek, R. Scheiber, L. M. H. Ulander, A. Gustavsson, G. Sandberg, S. Tebaldini, A. M. Guarnieri, F. Rocca, F. Bombardini, and M. Pardini. BioSAR 2007 technical assistance for the development of airborne SAR and geophysical measurements during the BioSAR 2007 experiment: Final report without synthesis. Technical report, ESA contract no. 20755/07/NL/CB, 2008.
- [4] P. Lopez-Dekker, F. De Zan, T. Borner, M. Younis, K. Papathanassiou, T. Guardabrazo, V. Bourlon, S. Ramongassie, N. Taveneau, L. M. H. Ulander, D. Murdin, N. Rogers, S. Quegan, and R. Franco. Biomass end-to-end mission performance simulator. In *IEEE International Geoscience and Remote Sensing Symposium (IGARSS)*, pages 4249–4252, Vancouver, BC, Canada, 24–29 July 2011.
- [5] L. G. Marklund. Biomassfunktioner för tall, gran och björk i Sverige. Rapport 45, Institutionen för skogstaxering, Sveriges lantbruksuniversitet, Umeå, Sweden, 1988.
- [6] G. T. Ruck, D. E. Barrick, W. D. Stuart, and C. K. Krichbaum. *Radar Cross Section Handbook*, volume 2. Plenum Press, 1970.
- [7] G. Sandberg, L. M. H. Ulander, J. E. S. Fransson, J. Holmgren, and T. Le Toan. L- and P-band backscatter intensity for biomass retrieval in hemiboreal forest. *Remote Sensing of Environment*, 115(11):2874–2886, 2011.
- [8] G. Sandberg, L. M. H. Ulander, J. Wallerman, and J. E. S. Fransson. Measurements of forest biomass change using P-band synthetic aperture radar backscatter. *IEEE Transactions on Geoscience and Remote Sensing*, 52(10):6047–6061, 2014.
- [9] M. J. Soja, H. J. Persson, and L. M. H. Ulander. Estimation of forest biomass from two-level model inversion of single-pass InSAR data. 2014. (submitted).
- [10] M. J. Soja, G. Sandberg, and L. M. H. Ulander. Regression-based retrieval of boreal forest biomass in sloping terrain using P-band SAR backscatter intensity data. *IEEE Transactions on Geoscience and Remote Sensing*, 51(5):2646–2665, 2013.
- [11] M. J. Soja and L. M. H. Ulander. A hybrid model for interferometric and polarimetric P-band SAR modelling of forests. In *Proceedings of PolInSAR 2011*, 2011. (ESA SP-695, March 2011).
- [12] M. J. Soja and L. M. H. Ulander. Polarimetric-interferometric boreal forest scattering model for BIOMASS end-to-end simulator. In *IEEE International Geoscience and Remote Sensing Symposium (IGARSS)*, pages 1061–1064, Quebec City, QC, Canada, July 13–18 2014.
- [13] F. T. Ulaby, D. Held, M. C. Dobson, K. C. McDonald, and T. B. A. Senior. Relating polarization phase difference of SAR signals to scene properties. *IEEE Transactions on Geoscience and Remote Sensing*, GE-25(1):83–92, January 1987.
- [14] L. M. H. Ulander, A. Gustavsson, B. Flood, D. Murdin, P. Dubois-Fernandez, X. Dupuis, G. Sandberg, M. J. Soja, L. E. B. Eriksson, J. E. S. Fransson, J. Holmgren, and J. Wallerman. BioSAR 2010: Technical assistance for the development of airborne SAR and geophysical measurements during the BioSAR 2010 experiment: Final report. Technical report, ESA contract no. 4000102285/10/NL/JA/ef, 2011.
- [15] P. Wikström, L. Edenius, B. Elfving, L. O. Eriksson, T. Lämäs, J. Sonesson, K. Öhman, J. Wallerman, C. Waller, and F. Klintebäck. The Heureka forestry decision support system: An overview. *Mathematical and Computational Forestry & Natural Resource Sciences*, 3(2):87–94, 2011.